Journal of Hazardous Materials, 11 (1985) 237—260
Elsevier Science Publishers B.V., Amsterdam — Printed in The Netherlands

MODELING THE PHASE I THORNEY ISLAND EXPERIMENTS

T.O. SPICER and J.A. HAVENS

University of Arkansas, Chemical Engineering Department, Fayetteville, Arkansas 72701 (U.S.A.)

(Received June 29, 1984; accepted November 15, 1984)

Summary

Laboratory experimental instantaneous releases of right circular cylindrical volumes of heavy gas mixtures (Freon-12/air) with initial volumes ranging from 0.034 m^3 to 0.135 m^3 and specific gravities ranging from 2.2 to 4.2 are described. Ground level peak gas concentrations are reported, and comparisons are made with corresponding 0.4 m elevation peak gas concentrations measured in Thorney Island Phase I Trials 7 through 16. An initial dilution phase in the Thorney trials immediately following release is observed which appears relatively unaffected by the ambient wind and which results in an order of magnitude dilution of the gas cloud. This initial phase of the Thorney Island trials, which prevails for lower wind speeds, is modeled accurately by the calm-air laboratory experiments at ~1:50 scale.

A mathematical model developed for incorporation in the U.S. Coast Guard Hazard Assessment Computer System (HACS) is described, and simulations of selected Thorney Island Phase I trials are compared with field measurements.

1. Introduction

We have been developing a general application, heavy gas dispersion model for incorporation in the U.S. Coast Guard Hazard Assessment Computer System (HACS) [1]. As part of the development, an extensive series of laboratory experimental heavy gas releases has been conducted. The laboratory experiments conducted to date have been instantaneous isothermal releases, in calm air, of right circular cylindrical volumes of dense gas. A primary purpose of these experiments has been to obtain accurate measurements of the lateral spreading rate and the associated turbulent mixing with air which is due to the rapid gravity-driven flow that ensues, and to investigate the scaling of such measurements for comparison (and prediction) of field releases.

Simultaneously with the laboratory release experiments, an extensive review has been made of the numerous mathematical model techniques which have been proposed. As a result of this review and an extensive program of mathematical model prediction comparisons with field data sets including the AGA LNG test series [2], the Esso/API LNG test series, the Burro

0304-3894/85/$03.30

and Coyote LNG test series [3,4], and the Shell Maplin Sands releases [5], as well as consideration of other small scale field and wind tunnel heavy gas dispersion data, we have concentrated on the modeling technique proposed for the Shell HEGADAS (HEavy GAs Dispersion from Area Sources) model. However, we have made substantial modifications to generalize the applicability of the model. In particular, we have modified the model to allow for air entrainment in the heavy gas cloud formation phase, and included energy balance effects associated with cloud/air mixture phase changes and heat transfer from the surface underlying the initially formed gas cloud.

This paper summarizes some of the results of our still-air laboratory release gas concentration measurements and compares them with measurements from the Thorney Island Phase I trials. We conclude that the laboratory and field tests demonstrate for this type of release the importance of an initial dilution phase during the period immediately following release. This dilution phase is relatively unaffected by the ambient wind and is accurately modeled by calm-air laboratory experiments at about 1:50 scale.

Finally, using air entrainment data obtained from the laboratory experiments to parameterize the mixing which occurs in the gravity spreading-controlled phase of the heavy gas cloud development, mathematical model predictions are compared with the measured downwind peak concentrations measured in Thorney Island Phase I Trials 7—9, 11, 13, and 15.

2. Laboratory model still-air tests

Our experimental facility has been designed for the instantaneous or time-dependent release of up to about 1 m^3 dense gas in the center of a flat 14.4 m diameter circular area. Simultaneous real-time gas concentration measurements are provided at up to eight positions anywhere in the spill area (including vertically to a height of about 1 m). Photographic documentation of smoke-marked releases utilizes motor-driven 35 mm cameras and a high speed 16 mm movie camera.

2.1 Release method

Figure 1 shows a sector of the release area surrounding a 135 liter gas container filled with white-smoke-marked Freon-12 gas with a height-to-diameter ratio one. The gas container is a 3 mm thick polycarbonate sheet rolled to form a cylinder with vertical exterior support ribs which extend above the cylinder to a fitting attached to the end of a rod in a pneumatic cylinder. The pneumatic cylinder is rigidly mounted in a framework hung from roof support beams. A solenoid valve operated by the computer control and data acquisition system admits air under the pneumatic cylinder piston for a designated time period, moving the gas container vertically past the gas volume.

The open-topped gas container is filled by introducing the test gas at the bottom through a distribution plate with eight radial outlets to minimize

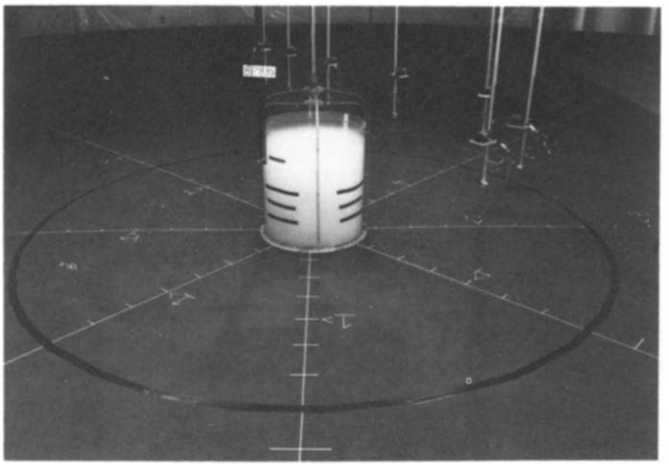

Fig. 1. 135 liter Freon-12, H/D = 1.0.

mixing effects due to gas jetting. Horizontal slots cut in the container wall determine the gas height when filled. The container removal time is controlled by the operating pressure of the air supply line and by the length of time the solenoid valve is maintained open, and measured by timing the passage of a reflective tape marker on the cylinder between light beams projected from optical fibers mounted to the side.

Container removal rates were studied using smoke-marked gas volumes to determine operating conditions required to leave a freestanding, minimally perturbed, cylindrical gas volume after the container had risen above the gas. Figure 2 shows high speed 16 mm movie frames of the vertical travel of the 135 liter container (H/D = 1.0) initially containing smoke-marked argon. The bottom of the container is past the top of the gas volume 0.18 seconds after its vertical movement began, and the second frame indicates that the gas is freestanding with essentially no movement or perturbation.

Figure 3 shows the (same view as Figure 1) spreading cloud taken 1.2 seconds after release. Figures 4 and 5 show overhead views of the release. In Figs. 4 and 5, the gas container is just hidden under the square plate which is part of the release mechanism framework. The edge of the spreading gas cloud has advanced to a radial distance of 1.5 m in Fig. 4 and 2.0 m in Fig. 5. The radial symmetry of the cloud is clearly indicated. Observations of the cloud's movement beyond the edges of the area photographed confirm radial cloud advance to distances at which the peak gas concentration at floor level has decreased to at least 1% of the initial value. The spreading gas rapidly forms a torus or doughnut shape, as observed in previous wind tunnel [6] and field [7] calm-air and low-wind releases.

2.2 Gas concentration measurement

In the background of Fig. 1 are shown vertical support rods on which gas sensors are mounted; sensors are positioned to avoid interference in the flow

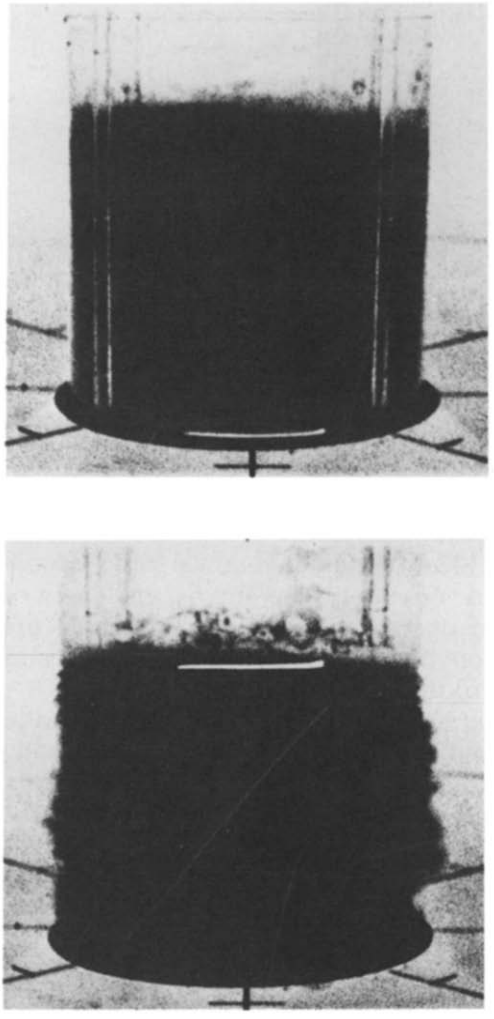

Fig. 2. Freestanding gas cylinder initial condition.

caused by other sensors. Figure 6 shows a sensor mounted on a support rod. A vacuum pump aspirates gas through a 4 mm diameter sample port fitted with a fibrous filter; the sample flows over a 4 μm wire or 25 μm film mounted on a TSI 1260 anemometer probe, and then through a 400 μm diameter choke. The aspiration rate with the 400 μm choke, used in most of the measurements described here, is approximately 1.5 liters/min, although some measurements have been made with aspiration rates as low as 300 ml/min. The high aspiration rates have been used to maximize the resolution of the peak concentrations in the cloud.

The hot wires or films were operated at overheat ratios of 1.32 and 1.16 respectively, corresponding to an operating temperature of about 85°C. This

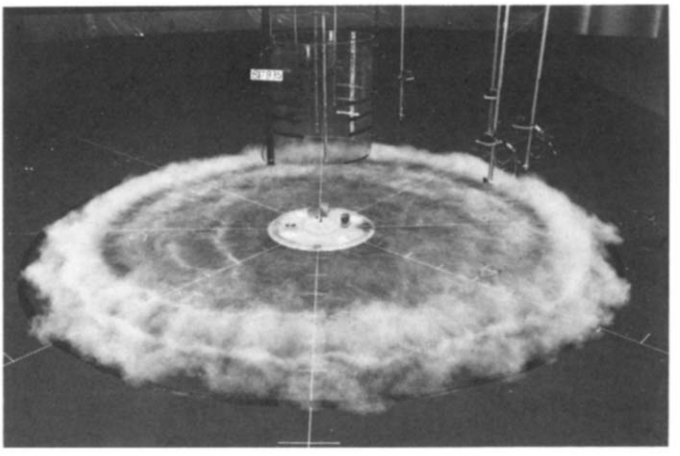

Fig. 3. 135 liter Freon-12 release, t = 1.2 s.

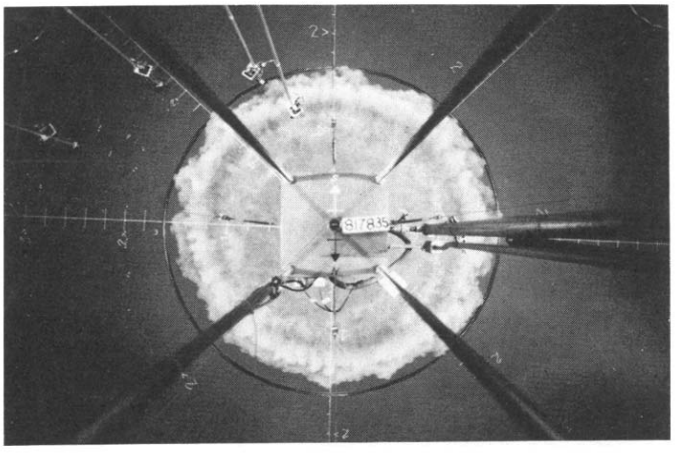

Fig. 4. 135 liter Freon-12 release, t = 1.2 s.

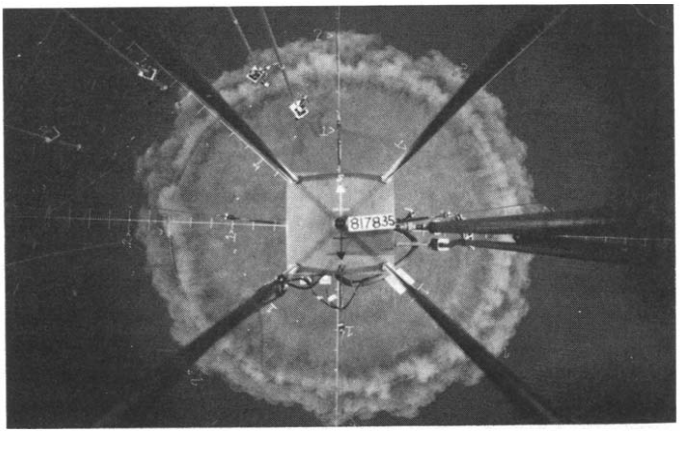

Fig. 5. 135 liter Freon-12 release, t = 1.7 s.

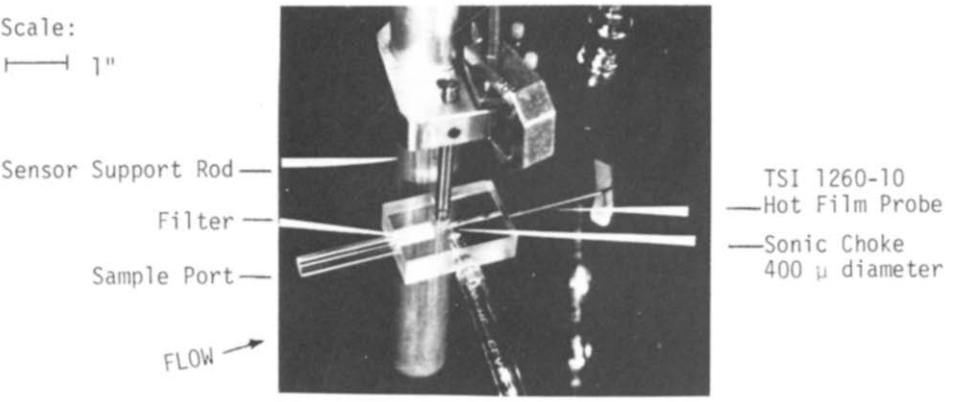

Fig. 6. Aspirated hot film gas concentration sensor.

operating condition was determined to give good resolution of the concentration of Freon-12/air mixtures without appreciable deterioration of the sensors experienced in high Freon-12 concentration, high overheat ratio usage. The output of the TSI 1053B anemometers is fed to a reference voltage shifting circuit, through a low pass filter (100 Hz) and amplifier, and input to a DEC MINC/11-23 computer data acquisition system. Gas concentration measurements were made at 250 Hz for 50 seconds after release.

Gas calibration mixtures are fed to the gas sensors just before filling the container and again at the end of a series of three repeat releases. Clear air readings are also made between releases to correct for sensor drift which may result primarily from change in air temperature or pressure and secondarily from other factors such as sensor aging and electronic circuitry drift. We estimate the gas concentration measurements reported to be accurate to within about 2% of reading in the range 50—100%, 4% of reading in the range 25—50%, 10% of reading in the range 5—25%, and 20% of reading in the area of 1% concentration, based on analysis of the sensor's drift characteristics. Primary standardization of the calibration mixtures prepared with rotameters was done by gas chromatography.

2.3 Test results

We summarize here measurements of the spreading and dilution of H/D = 1 Freon/air mixtures with volumes 34.2, 54.1, and 135 liters and specific gravities 2.15, 2.90, and 4.17. Each experimental release is repeated at least twice. Figure 7 shows typical ground level (0.6 cm) gas concentration measurements at three successive nondimensionalized radial distances ($R^* = R/V^{1/3}$) from the relase center. Three concentration time series, taken in three successive experiments, are shown for each radial position. In most cases, the variation of maximum concentrations is close to or within the expected accuracy of the concentration technique. Gas concentration measurements near the release indicate a complex, but remarkably repeatable,

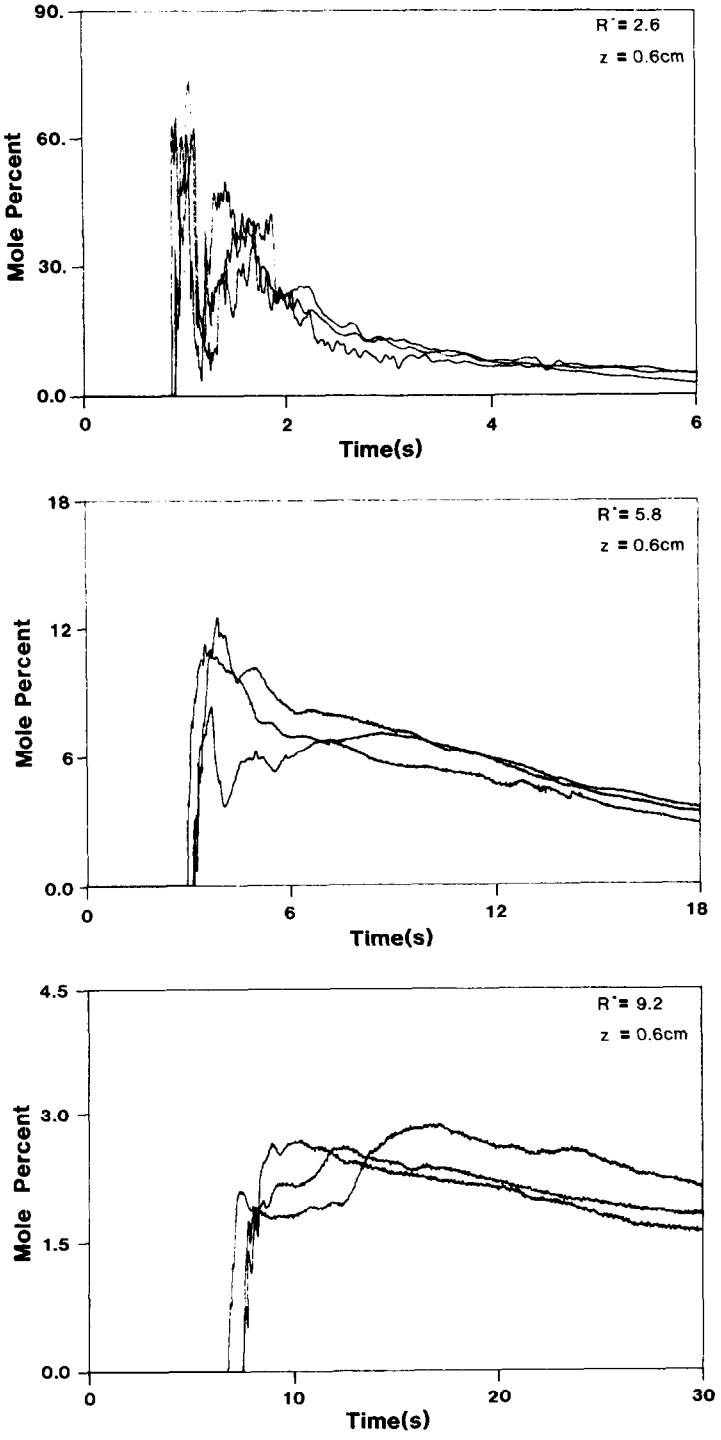

Fig. 7. Repeat gas concentration measurements at three radial positions, Freon-12, V = 0.054 m^3.

structure which appears to correlate well with complex flow patterns exhibited in the cloud leading edge near the release. Distinct peaks and valleys in the concentration records, as in Fig. 7, appear to correlate with observed complex roll and wave structures in the cloud's leading edge near the release (see Figs. 3—5). As the cloud spreads radially, the complex frontal movement is seen to diminish, both in the photographs and in the gas concentration measurements.

Hall et al. [6] have suggested that calm air releases of cubic volumes of gas should have a characteristic length of $l = V^{1/3}$ and a characteristic time scale $T = V^{1/6}/\sqrt{g\Delta}$ where g = gravitational acceleration and $\Delta = (\rho - \rho_a)/\rho_a$. Figure 8 shows peak measured gas mole fraction plotted against R^*, the non-dimensionalized distance from the spill center, for pure Freon-12 spills. The data for the three spill volumes collapse well using the scaling rules proposed by Hall et al. The individual points on Fig. 8 are averages of three repeat experimental runs, and the dashed lines define the outer boundaries on all peak concentrations measured for these releases. Figure 9 shows a plot of concentration vs. R^* for the three volumes tested, including releases with initial specific gravities 2.15, 2.90, and 4.17. All of the ground level peak concentration vs. dimensionless distance data taken for different volumes and initial densities fall within the same bounds as in Fig. 8 within the limits of experimental error and experiment reproducibility.

Figure 10 shows a plot of $t^* = t/T$, the non-dimensionalized cloud arrival time (measured from the concentration onset illustrated in Fig. 7) vs.

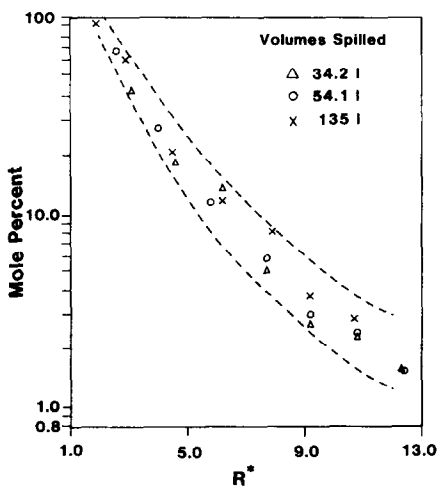

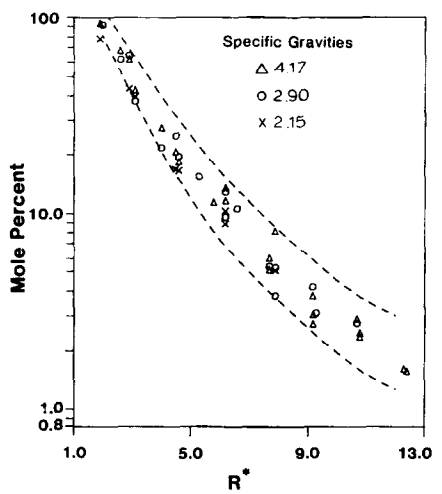

Fig. 8. Maximum concentration at $z = 0.6$ cm vs. R^*. Freon-12, 0.034, 0.054, and 0.135 m^3 volumes.

Fig. 9. Maximum concentration at $z = 0.6$ cm vs. R^*. Three gas volumes and three initial densities.

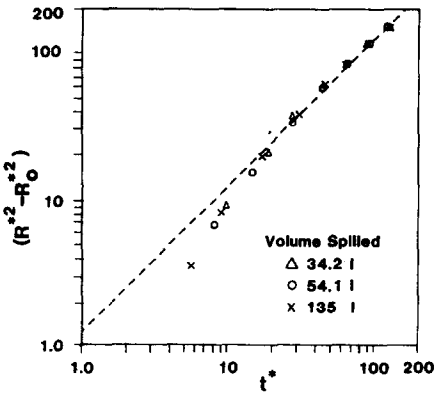

Fig. 10. Dimensionless distance vs. time of cloud arrival.

$(R^{*2} - R_0^{*2})$ for the three volumes tested. Integration of the "gravity intrusion" formula

$$dR/dt = C_E\sqrt{gH\Delta} \tag{1}$$

indicates that cloud radius should be proportional to $\sqrt{t}$. The line of slope 1 dashed on Fig. 10 corresponds to that dependence of R on t for times greater than $t^* \approx 20$. Extrapolation of the dashed line indicates a value of $C_E = 1.16$ in eqn. (1).

3. Comparison with Thorney Island test results

Table 1 summarizes the Phase I Thorney Island release conditions for Tests 7 through 16. We have not analyzed data from Tests 5 and 6 and 17, 18, and 19. Tests 7 through 16 are all essentially instantaneous releases of nominal 2000 m^3 volumes of Freon-12/air mixtures with initial height 13 m and diameter 14 m. The cloud dispersion process in these tests is initiated by a rapid gravity-driven flow phase in which the cloud slumps to the ground and spreads laterally. There is a characteristic time period following release in which the heavy gas flow field is relatively unaffected by the wind field. It follows that the initial dilution of the cloud will be relatively unaffected by the wind field, and should therefore be similar to a calm air release during this period. The extent of this period and the cloud dilution which occurs during this period as a result of turbulent mixing generated by the gravity-driven flow are important determinants of the maximum downwind distance reached by a given gas concentration level.

Figure 11 shows a plot of the maximum (peak) gas concentration measured at 0.4 m elevation along the centerline mean wind direction for Thorney Island Tests 7 through 16. We have superimposed on this plot the data bounding curves for our laboratory calm-air releases as summarized in Figs. 8 and 9. There is a clear indication of an initial dilution phase dom-

TABLE 1

Summary of Thorney Island Phase I trials Tests 7 through 16

Trial number	Initial specific gravity, ρ_0/ρ_A	Wind velocity (m/s) at 10 m	Initial Richardson number[a]	Ambient temperature (°C)	Relative humidity (%)	Pasquill stability
7	1.78	3.2	9.4	17.1	80.7	E
8	1.72	2.4	15	17.1	87.6	D
9	1.73	1.7	31	18.6	87.3	F
10	1.97	2.4	21	11.1	19.2	C
11	2.03	5.1	4.9	12.3	77.1	D
12	2.31	2.6	24	10.8	66.2	E
13	1.96	7.5	2.1	13.2	74.1	D
14	1.98	6.8	2.6	12.6	84.2	C/D
15	1.41	5.4	1.8	10.3	88.4	D
16	1.68	4.8	3.8	9.7	85.1	D

[a] $Ri_0 = g\left[\frac{\rho_0}{\rho_A} - 1\right] V^{1/3}/u_{10}^2$.

Note: The initial specific gravities for trial Nos. 7 to 14 were revised by NMI subsequent to the performance of this work. The revisions do not affect the conclusions.

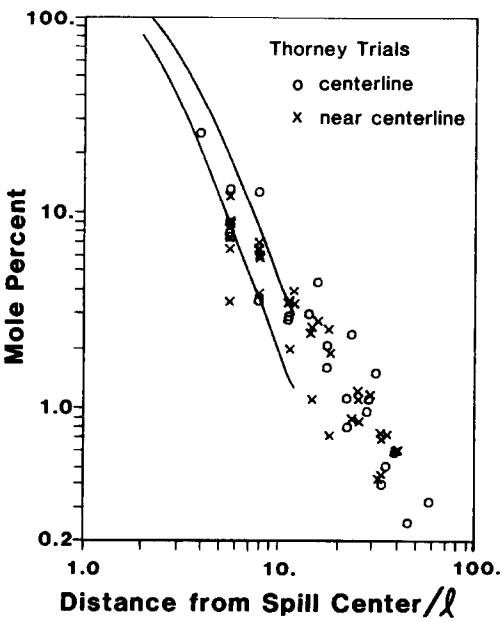

Fig. 11. Maximum cloud centerline, 0.4 m elevation, gas concentration measurements from Thorney Trials 7 through 17. Comparison with laboratory calm air releases.

inated by gravity-driven flow effects which is relatively unaffected by the ambient wind flow field. The duration of this initial phase, as would be expected, appears to be dependent on the initial release Richardson number, which reflects the relative strengths of the gravity-driven and ambient wind flows. During this time period the laboratory calm-air release results scale accurately to the Thorney Island 2000 m^3 release, representing a characteristic length scale factor increase of about 25. Furthermore, the initial gravity-driven dilution phase, for practical purposes, completely controls the maximum downwind distance to concentration levels as low as about 10% and appears to be the determining factor for concentration levels as low as 1%.

4. Mathematical model description

The model is an adaptation of the Shell HEGADAS model described by Colenbrander [8]. A lumped parameter model of the initial formation of a heavy gas "source" cloud, which incorporates air entrainment at the gravity spreading front using a frontal entrainment velocity, is substituted for the source description recommended for HEGADAS. The model is described in three parts: (a) The heavy gas source cloud formation, (b) the downwind dispersion model, and (c) the quasi-steady treatment of transient gas releases. The complete model is required for modeling the Thorney Island tests, although model capabilities which are being incorporated to account for effects of non-ambient temperature gas releases are not required.

4.1 Heavy gas source cloud formation

A "box" model of the initial formation of the heavy gas source cloud, which may form from an evaporating liquid pool or otherwise specified ground level emission source, or be an initially specified gas volume of prescribed dimensions for an instantaneous release, is illustrated in Fig. 12. The gas source cloud is represented as a cylindrical gas volume which spreads laterally as a density-driven flow, with entrainment *from* the top of the source cloud by wind shear and air entrainment *into* the advancing front edge. A mass balance on the total mass in the source cloud (M) gives

$$\frac{dM}{dt} = E(t) + \dot{M}_{a,e} - \pi R^2 Q^*_{max}/x_c \tag{2}$$

The rate of entrainment of air at the advancing cloud edge $\dot{M}_{a,e}$ is given by

$$\dot{M}_{a,e} = (2\pi RH)(\epsilon u)\rho_a \tag{3}$$

and the cloud edge (spreading) velocity is modeled as

$$u = \frac{dR}{dt} = C_E \left[g \left[\frac{\rho - \rho_a}{\rho} \right] H \right]^{1/2} \tag{4}$$

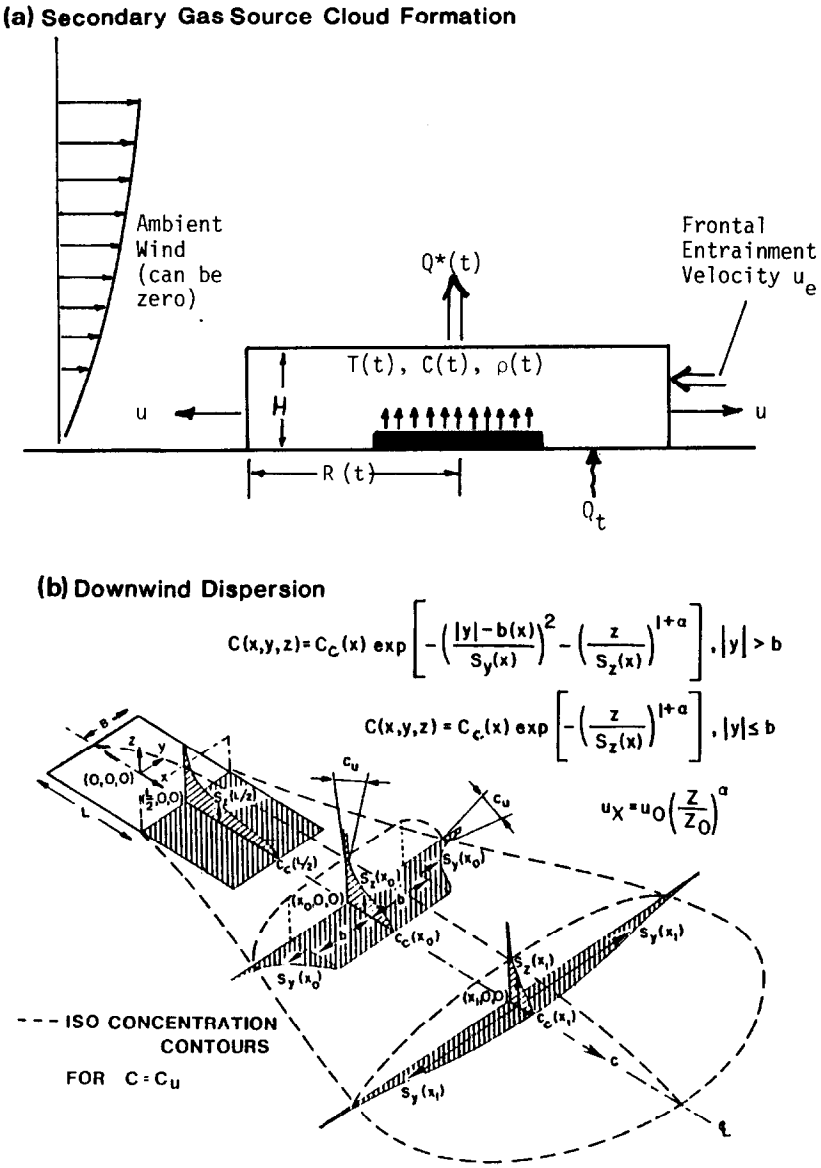

Fig. 12. Schematic diagram of recommended Coast Guard-HACS heavy gas dispersion model.

A mass balance on the air in the source cloud (M_a) gives

$$\frac{dM_a}{dt} = \dot{M}_{a,e} - \pi R^2 Q^*_{max} \left(\frac{x_a}{x_c}\right) \tag{5}$$

where $x_a = M_a/M$ is the mass fraction of air in the cloud.

The maximum atmospheric "takeup" rate of contaminant from the cloud top ($\pi R^2 Q^*_{max}$) is calculated from

$$Q^*_{max} = \frac{c_c u_0 S_z}{(1+\alpha)L}\left(\frac{S_z}{z_0}\right)^{\alpha} \tag{6}$$

where the flux is calculated based on a square source of equivalent area ($L^2 = \pi R^2$). S_z is specified by an analytical solution to the equation

$$\frac{d}{dx}\left[\left(\frac{S_z}{z_0}\right)^{1+\alpha}\right] = \frac{k}{z_0}\,\frac{u_*}{u_0}\,\frac{(1+\alpha)^2}{\phi(Ri_*)} \tag{7}$$

(See the subsequent section for the derivation of equations (6) and (7) and the specification of $\phi(Ri_*)$.)

Equations (2), (4) and (5) are integrated with respect to time, determining $M(t)$, $R(t)$, $M_a(t)$, and $Q^*(t)$. The source dimensions and the takeup rate ($\pi R^2 Q^*/x_c$) provide the initial conditions for the downwind dispersion calculation.

4.2 Downwind dispersion model

The model treats dispersion of gas entrained into the wind field from an idealized rectangular shape source of half width $y = B$ and length L. The idealized source results from the source cloud formation model described previously, with the (normally) circular source cloud represented as an equivalent area rectangle. The source is centered at $x = y = 0$ as shown in Fig. 12b. Similarity forms for the concentration profiles are assumed which represent the plume as being composed of a horizontally homogeneous section in which dispersion only occurs vertically, with Gaussian (concentration) profile edges. A power law wind velocity profile is assumed. With the assumed similarity forms for the concentration and velocity profiles, the variables c_c (ground level centerline gas concentration), b (width of the horizontally homogeneous center section of the plume), and S_y and S_z (scale factors in the similarity forms for concentration) are constrained by ordinary differential equations.

$S_z(x)$ is determined by requiring that it satisfy the diffusion equation

$$u_x \frac{\partial c}{\partial x} = \frac{\partial}{\partial z}\left[K_z \frac{\partial c}{\partial z}\right] \tag{8}$$

with a vertical turbulent diffusivity given by

$$K_z = \frac{k u_* z}{\phi(Ri_*)} \tag{9}$$

The function $\phi(Ri_*) = 0.74 + 0.25\,Ri_*^{0.7} + 1.2 \times 10^{-7}\,Ri_*^3$, proposed by Colenbrander, is a curve fit of laboratory scale data for vertical mixing in

stably density-stratified fluids reported by McQuaid [9] and Kantha et al. [10]. The friction velocity in eqn. (9) is calculated assuming a logarithmic wind velocity profile

$$u_* = k u_0 \left[\ln \left(\frac{z_0 + z_r}{z_r} \right) - \psi_1 \left(\frac{z_0}{\lambda} \right) \right]^{-1} \tag{10}$$

Combining the assumed similarity forms for concentration and wind velocity with eqns. (8)—(10) gives

$$\frac{\mathrm{d}(S_z/z_0)^{1+\alpha}}{\mathrm{d}x} = \frac{k}{z_0} \frac{u_*}{u_0} \frac{(1+\alpha)^2}{\phi(Ri_*)} \tag{11}$$

where the Richardson number is computed as

$$Ri_* = g \frac{\rho(c_c) - \rho_a(H_{eff})}{\rho_a(z=0)} \frac{H_{eff}}{u_*^2} \tag{12}$$

and the effective cloud depth is defined as

$$H_{eff} = \frac{1}{c_c} \int_0^\infty c \, \mathrm{d}z = \frac{\Gamma(1/(1+\alpha))}{1+\alpha} S_z \tag{13}$$

Equation (11), which is derived for two-dimensional dispersion, is "generalized" to the following form for application to a heavier-than-air gas plume as a density intrusion:

$$\frac{\mathrm{d}}{\mathrm{d}x} \left[B_{eff} \left(\frac{S_z}{z_0} \right)^{1+\alpha} \right] = \frac{k}{z_0} \frac{u_*}{u_0} \frac{(1+\alpha)^2 B_{eff}}{\phi(Ri_*)} \tag{14}$$

where the plume "effective half width" is defined by

$$B_{eff} = b + \frac{\sqrt{\pi}}{2} S_y \tag{15}$$

and determined using the gravity intrusion relation [11,12]

$$\frac{\mathrm{d}B_{eff}}{\mathrm{d}t} = \sqrt{g \left(\frac{\rho(c_c) - \rho_a(z=0)}{\rho(c_c)} \right) H_{eff}} \tag{16}$$

The average transfer velocity in the plume can be shown to be

$$u_{eff} = u_0 (S_z/z_0)^\alpha (\Gamma(1/(1+\alpha)))^{-1} \tag{17}$$

and it follows that

$$\frac{\mathrm{d}B_{eff}}{\mathrm{d}x} = C' \sqrt{1 - \frac{\rho_a(z=0)}{\rho(c_c)}} \left(\frac{S_z}{z_0} \right)^{(1/2-\alpha)} \tag{18}$$

with

$$C' = \left(\frac{g z_0 \Gamma^3 (1/(1+\alpha))}{u_0^2 (1+\alpha)} \right)^{1/2}$$

The crosswind similarity parameter $S_y(x)$ is also determined by requiring that it satisfy the diffusion equation

$$u_x \frac{\partial c}{\partial x} = \frac{\partial}{\partial y} K_y \frac{\partial c}{\partial y} \tag{19}$$

with the horizontal turbulent diffusivity given by

$$K_y = K_0 u_x B_{\text{eff}}^{\gamma} \tag{20}$$

When $b = 0$, $S_y = \sqrt{2}\sigma_y$, where σ_y is the similarity parameter correlated by Pasquill—Gifford [13] as $\sigma_y = \delta x^{\beta}$ for use in the relation

$$c = c_c \exp\ (-\tfrac{1}{2}(y/\sigma_y)^2) \tag{21}$$

Further, when $b = 0$ eqns. (19)—(21) require that

$$\sigma_y \frac{d\sigma_y}{dx} = K_0 B_{\text{eff}}^{\gamma} \tag{22}$$

with $\gamma = 2 - 1/\beta$ and $K_0 = (2\beta/\pi)(\delta\sqrt{\pi/2})^{1/\beta}$. Thus

$$S_y \frac{dS_y}{dx} = \frac{4\beta}{\pi} B_{\text{eff}}^2 \left\{ \frac{\delta\sqrt{\pi/2}}{B_{\text{eff}}} \right\}^{1/\beta} \tag{23}$$

Equation (23) is also generalized at this point by assuming it applicable when determining S_y even when b is not zero.

At a downwind distance x_t where b has decreased to zero, the crosswind concentration profile is assumed Gaussian with S_y given by

$$S_y = \sqrt{2}\delta (x + x_v)^{\beta} \tag{24}$$

where x_v is a virtual source distance given by

$$S_y(x_t) = \sqrt{2}\delta (x_t + x_v)^{\beta} \tag{25}$$

It is assumed that gravity spreading is terminated for $x > x_t$.

For a steady gas/air plume, the center line concentration c_c is determined from the material balance

$$E = \int_0^{\infty} \int_{-\infty}^{\infty} c u_x \, dy \, dz = \frac{2 c_c u_0 S_z^{1+\alpha} B_{\text{eff}}}{(1+\alpha) z_0^{\alpha}} \tag{26}$$

where E is the plume gas source strength.

Equations (11)—(15), (18) and (23)—(26) are combined with an equation of state relating cloud density to gas concentration and are solved simultaneously to predict S_z, S_y, c_c, and B_{eff} as functions of downwind distance beginning at the downwind edge of the gas source.

In the event that $E(t)$, the gas evolution rate from the primary source, is less than the potential atmospheric takeup rate, no gas source accumulation occurs. The source length and half-width are then $L = L_p$ and $B = B_p$, and for an average value of the ground level concentration $\tilde{c}_c$,

$$Q^* = \frac{\tilde{c}_c u_0 (S_{z_0})^{1+\alpha}}{(1+\alpha) z_0^{\alpha} L} \tag{27}$$

In this case, eqn. (27) must be solved by iteration, since the values of $\tilde{c}_c$ and S_z are related through the concentration dependence of the Richardson number. S_{z_0}, the value of S_z at the downwind edge of the heavy gas source, is computed using eqn. (11) over the source, starting with $S_z = 0$ at the upwind edge of the source, and neglecting lateral dispersion over the source.

4.3 Quasi-steady approximate treatment of transient gas releases

The model provides for treatment of transient gas releases, i.e., releases in which the area of the gas source and/or the gas emission rate vary with time. The dispersion downwind of such releases is computed for a series of source configurations representing the time-varying primary source. Information from this series of steady state predictions is then extracted to provide a quasi-steady state description of the transient dispersion downwind of the source.

Following Colenbrander's description [8], consider a series of "observers" travelling (in the wind field) over the transient gas source which is assumed circular with radius $R(t)$ and vertical emission (flux) $Q^*(t)$. The vertical vapor flux is assumed spatially uniform over the source. The transient gas source is represented as an equivalent square shape with length $L(t) = \sqrt{\pi} R(t)$. If $Q(t) < Q^*_{max}(L_p(t))$, then $B(t) = B_p(t)$ and $Q^*(t) = Q(t)$. The ground level concentration at the source downwind edge is determined as indicated in eqn. (27). If $Q(t) > Q^*_{max}(L(t))$, a heavy gas source cloud accumulates over the gas source. The heavy gas source cloud is assumed cylindrical in shape with radius $R(t)$ and height $H(t)$, and is modeled as described in the previous section on the heavy gas cloud formation phase, resulting in specification of the time-varying source cloud radius, $R(t)$, and contaminant takeup rate $Q^*(t)\pi R^2(t)$.

Let the subscript i refer to quantities associated with "observer" i. Consider that the observers originate from the point which corresponds to the maximum upwind extent of the gas layer ($x = -R_{max}$).

The desired observer velocity is the average transport velocity of the gas u_{eff}; however, the value of u_{eff} will differ from observer to observer with the unfortunate consequence that some observers may be overtaken by others. If

one examines a neutrally buoyant cloud, the value of u_{eff} becomes a function of downwind distance alone. With this functionality and the value of S_{z_0} when the averaged source rate ($\pi R^2 Q^*$) is a maximum (denoted with the subscript m), Colenbrander models the observer velocity to be:

$$u_i(x) = \frac{u_0}{\Gamma\left(\frac{1}{1+\alpha}\right)} \left[\frac{S_{z_{0m}}}{z_0}\right]^{\alpha} \left\{\frac{x + R_{\max}}{\frac{\sqrt{\pi}}{2} R_m + R_{\max}}\right\}^{\alpha/(1+\alpha)} \tag{28}$$

Noting that $u_i(x) = dx/dt$, observer position and velocity as functions of time are determined.

A time-averaged source as seen by each observer is computed. If t_{up_i} and t_{dn_i} denote the times when observer i encounters the upwind and downwind edges of the source, respectively, then the source length seen by observer i is:

$$L_i = x_i(t_{dn_i}) - x_i(t_{up_i}) \tag{29}$$

The half width of the source, $B_i'(t)$, is:

$$B_i'(t) = \sqrt{R^2(t) - x_i^2(t)} \tag{30}$$

Consequently, the gas source "half area" A_i seen by the observer is given by

$$A_i = \int_{t_{up_i}}^{t_{dn_i}} u_i(t) B_i'(t)\, dt \tag{31}$$

An average observed half width (required for representing the source as rectangular) is given by

$$B_i = A_i/L_i\,, \tag{32}$$

and the average takeup flux from the gas source during the passage of observer i is given by

$$Q_i^* = \frac{\int_{t_{up_i}}^{t_{dn_i}} Q^*(t) B_i'(t) u_i(t)\, dt}{B_i L_i} \tag{33}$$

In order to close the integral material balance (equation (26)) over the source, an averaged value of $S_{z_{0i}}$ is calculated:

$$S_{z_{0i}} = \int_{t_{up_i}}^{t_{dn_i}} \left(\frac{dS_z}{dx}\right) u_i(t)\, dz \tag{34}$$

where dS_x/dx is substituted from eqn. (11). Unfortunately, this method of

determining S_{z_0} can result in values of c_c computed from the material balance (equation (26)) which exceed ρ_E. When this occurs, the value of S_{z_0} is calculated with the integral material balance and ρ_E.

For each of several observers, released successively from $x = -R_{max}$, the observed dimensions L_i and B_i, the upwind and downwind edges of the observed source, the average vertical dispersion coefficient, $S_{z_{0i}}$, and the average takeup flux Q_i^* applicable during the observer's passage can be determined. For each such observer, a steady state calculation of $c_{c_i}(x)$, $S_{y_i}(x)$, $S_{z_i}(x)$, and $B_i(x)$ is made.

The concentration distribution at any specified time t_s is then determined by locating the position of the series of observers at time t_s, i.e. $x_i(t_s)$, and noting that quasi-steady values of the concentration, S_y, S_z, and b at times t_s are $c_c(x_i(t_s))$, $S_y(x_i(t_s))$, $S_z(x_i(t_s))$, and $b(x_i(t_s))$. The corresponding concentration distribution is then computed from the assumed profiles given in Fig. 12.

4.4 Allowance for dispersion along the wind direction

Following Colenbrander, we also apply a "correction" or adjustment to the values of c_c calculated as described above to account for dispersion in the wind direction. The calculated ground level concentration $c_c(x)$ is considered to have resulted from the release of successive planar puffs of gas ($c_c(x)\Delta x$) without any dispersion in the x-direction. If it is assumed that each puff diffuses in the x-direction as the puff moves downwind independently of any other puff and that the dispersion is one-dimensional and Gaussian, the x-direction concentration dependence is given by

$$c_c'(x; x_{p_i}) = \frac{c_c(x_{p_i})\Delta x_i}{\sqrt{2\pi}\sigma_x} \exp\left\{-\tfrac{1}{2}\left(\frac{x - x_{p_i}}{\sigma_x}\right)^2\right\} \tag{35}$$

where x_{p_i} denotes the position of the puff center due to observer i.

The x-direction dispersion coefficient σ_x is assumed to be a function of distance from the downwind edge of the gas source ($x - x_0$) and atmospheric stability given by

$$\begin{aligned}
\sigma_x(x - x_0) &= 0.02(x - x_0)^{1.22} \quad \text{for } \frac{1}{\lambda} < 0 \text{ (unstable)}; \quad x - x_0 \geqslant 130 \\
&= 0.04(x - x_0)^{1.14} \quad \text{for } \frac{1}{\lambda} = 0 \text{ (neutral)}; \quad x - x_0 \geqslant 100 \\
&= 0.17(x - x_0)^{0.97} \quad \text{for } \frac{1}{\lambda} > 0 \text{ (neutral)}; \quad x - x_0 \geqslant 50
\end{aligned} \tag{36}$$

where $(x - x_0)$ and σ_x are in meters [14]. The concentration at x is then determined by superposition, i.e., the contribution to c_c' at a given x from neighboring puffs is added to give an x-direction corrected value of c_c. For N observers,

$$c'_c(x) = \sum_{i=1}^{N} \frac{c_c(x_{pi})}{\sqrt{2\pi}\sigma_x} \exp\left[-\tfrac{1}{2}\left(\frac{x - x_{pi}}{\sigma_x}\right)^2\right] \Delta x_i \tag{37}$$

and for large N,

$$c'_c(x) = \frac{1}{\sqrt{2\pi}} \int_0^{\infty} \frac{c_c(\zeta)}{\sigma_x(\zeta - \zeta_0)} \exp\left\{-\tfrac{1}{2}\left[\frac{x - \zeta}{\sigma_x(\zeta - \zeta_0)}\right]^2\right\} d\zeta \tag{38}$$

5. Mathematical model simulation of Thorney Island Phase I tests

Trials 7 through 9, 11, 13 and 15, which represent the maximum range of wind velocity as well as initial spill Richardson numbers for the Phase I trials (including Trials 5, 6 and 17 through 19, which we have not analyzed) have been simulated using the model described previously.

The model input conditions used for the simulations are taken from Table 1. The model requires as input the volume to be released and its dimensions, the initial density (gas concentration), wind velocity at specified height, ambient temperature, pressure and humidity, Pasquill stability category, and surface roughness. For all simulations, a 2000 m^3 source, 14 m diameter, and 13 m height were used, as was a site surface roughness of 0.01 m.

Figures 13 through 18 show the model computed centerline maximum (peak) concentration vs. downwind distance. The first, straight-line section represents the computed heavy gas source cloud concentration, and the

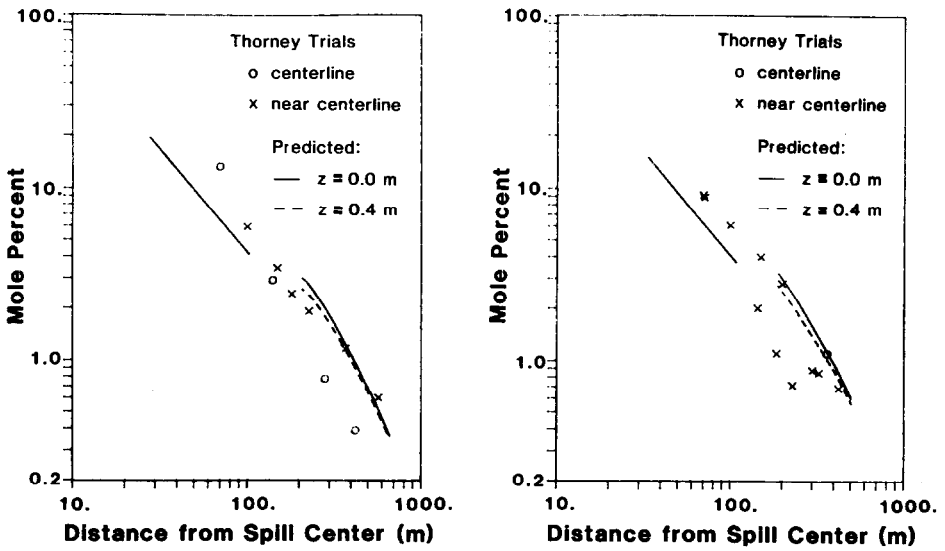

Fig. 13. Maximum concentration vs. distance for trial No. 7.

Fig. 14. Maximum concentration vs. distance for trial No. 8.

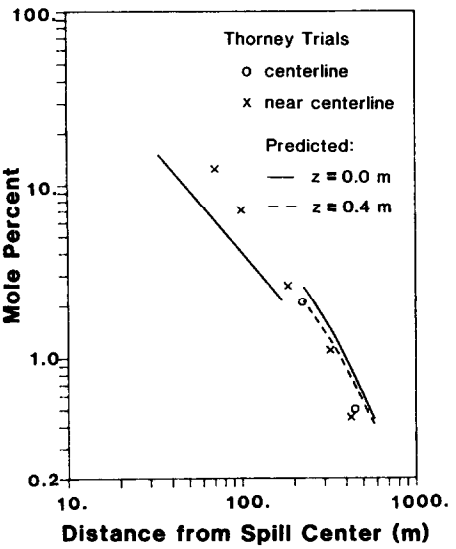

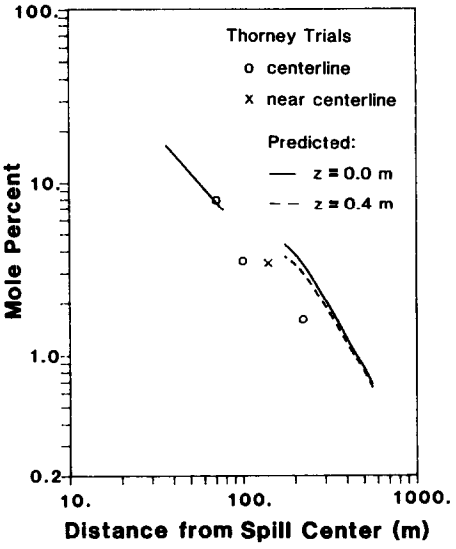

Fig. 15. Maximum concentration vs. distance for trial No. 9.
Fig. 16. Maximum concentration vs. distance for trial No. 11.

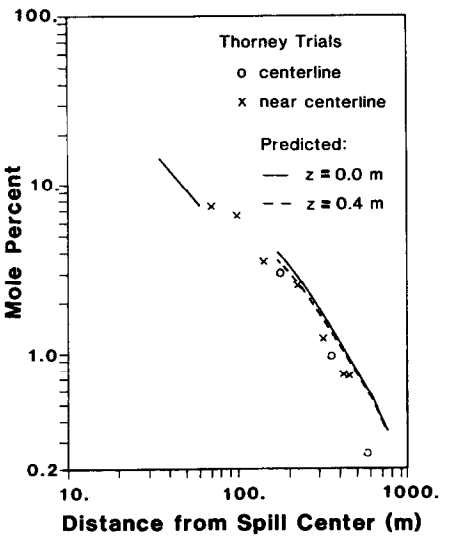

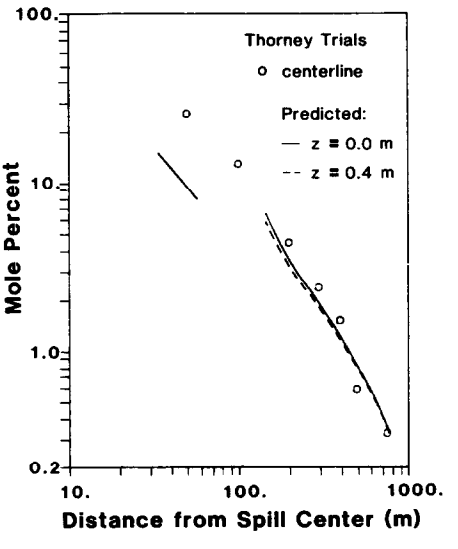

Fig. 17. Maximum concentration vs. distance for trial No. 13.
Fig. 18. Maximum concentration vs. distance for trial No. 15.

downwind extent of this line indicates the limit of the computed gravity spread of the source cloud. The computed concentration in this region represents a cloud volume average concentration and reflects the use of a frontal entrainment coefficient of 0.6 (see equation (3)) which is tentatively rec-

ommended from our analysis of the laboratory calm-air experiments described earlier. The experimental data shown represent the maximum measured values (0.6 s time average) observed at stations located on the centerline mean wind direction and at the nearest stations on either side thereof. Concentrations measured at stations on the mean wind direction centerline are designated.

The results shown in Figs. 13 through 18 collectively indicate a predicted maximum downwind distance to the 1% gas concentration level which agrees with the experimental field measurements to within about 20% for all of the release conditions represented, which encompasses essentially all of the Thorney Island test variable range except that of the pure Freon-12 release in Test No. 17. Uncertainty in the specification of atmospheric stability and the appropriate representation of the site surface roughness, as well as variations in the wind speed and direction around the mean values used for the simulation can account for differences as great as those shown between predictions and measurements. Consequently, we believe the simulation results are sufficiently accurate to justify the use of this model for prediction of the maximum concentration versus distance expected for releases of this type.

6. Conclusions

Analysis of gas concentration measurements from Thorney Island trials Nos. 7—16, representing nominal 2000 m^3 Freon/air instantaneous releases with initial aspect ratio approximately one, initial specific gravities ranging from 1.41 to 2.31, wind speeds at 10 m height ranging from 1.7 to 7.5 m/s, and atmospheric stabilities ranging from slightly unstable to stable, indicates that *for this type of release*:

(i) There is a characteristic time following release during which the heavy gas flow and the associated dilution with air are relatively unaffected by the wind field.

(ii) Comparison with our laboratory experimental calm-air instantaneous release results indicates that the initial dilution phase of the Thorney Island trials is accurately modeled at laboratory scale (~1:50). This initial dilution phase is indicated to extend to a nondimensional time of about 40 at which time the maximum cloud concentration at the advancing front is about 10%. The rapid dilution occurring during this phase continues to be an important factor in determining the time scale and distance at which maximum concentration in the cloud have reduced to the 1% level characteristic of fuel—air lower flammability limits.

(iii) The presence of wind increases the maximum downwind distance to concentration levels of the order of 1%. Although a correlation of this distance with the cloud initial density and wind velocity appears to be indicated, we have not yet drawn any conclusions in this regard.

(iv) A mathematical model, adapted from the Shell HEGADAS model

described by Colenbrander [8], modified to incorporate a heavy gas source formation phase which accounts for air entrainment at the advancing gravity-driven gas current front, and utilizing an air entrainment coefficient specification based on the results of our laboratory still-air heavy gas release experiments has been developed. The model predicts the maximum (peak) concentrations vs. distance observed in the simulated trials sufficiently accurately to justify the model's use for prediction of heavy gas peak concentration decay with distance expected for releases of this type.

Acknowledgements

The authors gratefully acknowledge the support of the U.S. Coast Guard Office of Research and Development and the Gas Research Institute through Contract DTCG23-80-C-20029.

Notation

A_i source area seen by observer i (m^2)
B source half width (m)
B_i' local half width of source seen by observer i (m)
B_{eff} effective width of gas plume (m)
B_p primary source half width (m)
b half width of horizontally homogeneous central section of gas plume (m)
c concentration (kg/m^3)
c_c centerline, ground level concentration (kg/m^3)
c_c' centerline concentration corrected for x-direction dispersion (kg/m^3)
$\tilde{c}_c$ average ground level concentration (kg/m^3)
C_E constant in density intrusion (spreading) relation
E source rate (kg/s)
g acceleration of gravity (m^2/s)
H height or depth of density intrusion or cloud (m)
H_{eff} effective cloud depth, eqn. (13) (m)
K_0 constant in eqn. (20) ($m^{1-\gamma}$)
K_y horizontal turbulent diffusivity (m^2/s)
K_z vertical turbulent diffusivity (m^2/s)
k von Karman's constant, 0.35
L source length (m)
L_p primary source length (m)
l characteristic length, $V^{1/3}$
M total cloud mass (kg)
M_a total air in the cloud (kg)
$\dot{M}_{a,e}$ mass rate of air entrainment into the cloud (kg/s)
N number of observers
Q gas source flux from primary source (kg/m^2 s)

Q^* atmospheric takeup flux (kg/m^2 s)
Q^*_{max} maximum atmospheric takeup flux (kg/m^2 s)
R gas source cloud radius (m)
R_m value of R when ($\pi R^2 Q^*$) is a maximum (m)
R_{max} maximum radius of the cloud (m)
R_p primary source radius (m)
R^* nondimensionalized radius, R/l
Ri_0 initial Richardson number, Thorney Island trials
Ri_* Richardson number, eqn. (12)
S_y horizontal concentration scaling parameter (m)
S_z vertical concentration scaling parameter (m)
S_{z_0} S_z at the downwind edge of the source ($x = L/2$) (m)
$S_{z_0 m}$ value of S_{z_0} when ($\pi R^2 Q^*$) is a maximum (m)
t time (s)
T characteristic time (s)
t_{dn_i} time when observer i encounters downwind edge (s)
t_{up_i} time when observer i encounters upwind edge (s)
t^* nondimensional time t/T
u cloud edge gravity spreading velocity (m/s)
u_i velocity of observer i (m/s)
u_x wind velocity, along x-direction (m/s)
u_0 wind velocity measured at $z = z_0$ (m/s)
u_{10} wind velocity at $z = 10$ m (m/s)
u_{eff} effective cloud advection velocity (m/s)
u_* friction velocity (m/s)
V initial volume of release (m^3)
x,y,z Cartesian coordinates (m)
x_0 downwind position of the gas source (m)
x_a, x_c mass fraction air and contaminant, respectively
x_{pi} position of puff center due to observer i (m)
x_t downwind distance where gravity spreading terminates (m)
x_v virtual point source distance (m)
z_0 reference height in wind velocity profile specification (m)
z_r surface roughness (m)

α constant in power law wind profile
β constant in σ_y correlation
γ constant in eqn. (20)
Γ gamma function
δ constant in σ_y correlation (m)
Δ non-dimensional density $(\rho - \rho_a)/\rho_a$
ϵ frontal entrainment coefficient in eqn. (4)
ρ density of gas—air mixture (kg/m^3)
ρ_0 initial density of gas—air mixture (kg/m^3)
ρ_a density of air (kg/m^3)

ρ_E density of emitted gas (kg/m^3)
σ_x x-direction dispersion coefficient (m)
σ_y Pasquill—Gifford lateral dispersion coefficient (m)
$\phi(Ri_*)$ function describing influence of stable density stratification on vertical diffusion
Ψ_1 stability correction to logarithmic velocity profile
λ Monin—Obukhov length (m)

References

1 U.S. Coast Guard Contract DTCG23-80-C-20029. Development of Vapor Dispersion Models for Non-Neutrally Buoyant Gas Mixtures, with the University of Arkansas, J.A. Havens, Principal Investigator.
2 American Gas Association Project IS-3-1, LNG Safety Program, Interim Report on Phase II Work, July 1, 1974, Battelle Columbus Laboratories.
3 R.P. Koopman, J. Baker, R.T. Cederwall, H.C. Goldwire, Jr., W.J. Hogan, L.M. Kamppinen, R.D. Kiefer, J.W. McClure, T.G. McRae, D.L. Morgan, L.K. Morris, M.W. Spann, Jr. and C.D. Lind, Burro Series Data Report (1981), LLNL/NWC 1980 LNG Spill Tests, Lawrence Livermore National Laboratories, Livermore, California.
4 H.C. Goldwire, Jr., H.C. Rodean, R.T. Cederwall, E.J. Kansa, R.P. Koopman, J.W. McClure, T.G. McRae, L.K. Morris, L. Kamppinen, R.D. Kiefer, P.A. Urtiew and C.D. Lind, Coyote Series Data Report (1981), LLNL/NWC 1981 LNG Spill Tests, Lawrence Livermore National Laboratories, Livermore, California.
5 J.S. Puttock, D.R. Blackmore and G.W. Colenbrander, Field experiments on dense gas dispersion, J. Hazardous Materials, 6 (1+2) (1982) 13—41.
6 D.J. Hall, E.J. Hollis and H. Ishaq, A Wind Tunnel Model of the Porton Dense Gas Spill Field Trials, LR 394 (AP), Warren Spring Laboratory, Department of Industry, Stevenage, UK.
7 R.G. Picknett, Field Experiments on the Behavior of Dense Clouds, Chemical Defence Establishment Report PTN, IL 1154/78/1, Porton Down, UK, September 1978.
8 G.W. Colenbrander, A mathematical model for the transient behavior of dense vapor clouds, 3rd International Symposium on Loss Prevention and Safety Promotion in the Process Industries, Basel, Switzerland, 1980.
9 J. McQuaid, Some experiments on the structure of stably stratified shear flows, Technical Paper P21, Safety in Mines Research Establishment, Sheffield, UK, 1976.
10 L.H. Kantha, O.M. Phillips and R.S. Azad, On turbulent entrainment at a stable density interface, J. Fluid Mechanics, 79 (1977) 753—768.
11 C.S. Yih, Dynamics of Non-Homogeneous Fluids, Macmillan, New York, 1965.
12 J.S. Turner, Buoyancy Effects in Fluids, Cambridge University Press, 1973.
13 F. Pasquill, Atmospheric Diffusion, Halsted Press Division of John Wiley and Sons, Inc., New York, 1974.
14 G.A. Beals, Guide to Local Diffusion of Air Pollutants, Technical Report 214, Air Weather Service, USAF, May 1971, NTIS, AD 726984.